NANO LETTERS

Letter

pubs.acs.org/NanoLett

Manipulation and Confinement of Single Particles Using Fluid Flow

Melikhan Tanyeri[†] and Charles M. Schroeder*[,†,‡,§]

[†]Department of Chemical and Biomolecular Engineering, [‡]Department of Materials Science and Engineering, and [§]Center for Biophysics and Computational Biology, University of Illinois at Urbana−Champaign, Urbana, Illinois 61801, United States

Supporting Information

ABSTRACT: High precision control of micro- and nanoscale objects in aqueous media is an essential technology for nanoscience and engineering. Existing methods for particle trapping primarily depend on optical, magnetic, electrokinetic, and acoustic fields. In this work, we report a new hydrodynamic flow based approach that allows for fine-scale manipulation and positioning of single micro- and nanoscale particles using automated fluid flow. As a proof-of-concept, we demonstrate trapping and two-dimensional (2D) manipulation of 500 nm and 2.2 μm diameter particles with a positioning precision as small as 180 nm during confinement. By adjusting a single flow parameter, we further show that the shape of the effective trap potential can be efficiently controlled. Finally, we demonstrate two distinct features of the flow-based trapping method, including isolation of a single particle from a crowded particle solution and active control over the surrounding medium of a trapped object. The 2D flow-based trapping method described here further expands the micro/nanomanipulation toolbox for small particles and holds strong promise for applications in biology, chemistry, and materials research.

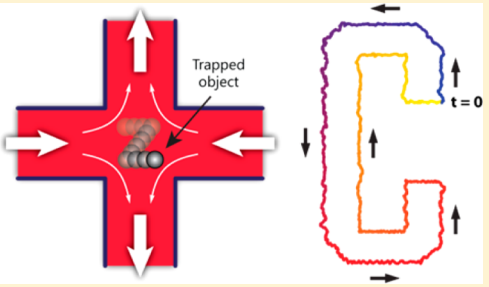

KEYWORDS: *Micro- and nanomanipulation, tweezers, trapping, hydrodynamic trap, microfluidics*

Precise methods for particle confinement and manipulation have played a major role in advancing basic and applied science during the past three decades.[1−3] In particular, fine-scale control over the position of colloidal particles in liquid medium has enabled comprehensive studies of fundamental problems in physics, chemistry, biology, and materials science. For this purpose, a wide range of methods have been developed utilizing forces based on optical,[4−23] electrical,[24−39] magnetic,[40−42] and acoustic[43−46] potential fields. Despite the demonstrated benefits and versatility of these methods, new approaches to particle manipulation are required to study fundamental problems in biophysics (e.g., protein folding or biomolecular conformational dynamics), soft matter (e.g., single polymer dynamics), and biology (e.g., single cell mechanics).

Among the existing methods for trapping, optical confinement techniques are arguably the most established and versatile, offering high precision control of micro- and nanoscale objects.[4−23] Conventional optical tweezers are based on tightly focused laser beams exerting strong optical gradient forces to confine objects. For these methods, the tightness of confinement scales with the volume of the object, which imposes a lower limit on the particle size for a given laser power.[47] To address this challenge, plasmonic and optofluidic nanotweezers have been recently developed.[14−23] These methods capitalize on amplified electromagnetic fields around specifically designed nanostructures, thereby enabling optical trapping of small molecules and nanoparticles (<50 nm) without substantially raising the temperature of the surrounding medium.[16]

A recent promising approach for particle confinement has been developed based on feedback-controlled electric fields.[29−37] Pioneered by Shapiro et al. and Cohen et al., electrokinetic trapping functions by observing the position of a particle and uses a feedback control mechanism to apply a two-dimensional (2D) corrective electrokinetic flow, which induces a drift to direct the particle to a desired position. In this way, a combination of electrophoretic forces and electroosmotic flows are used to manipulate particles. Using this method, Shapiro et al. demonstrated positioning precision of ∼50 nm (during confinement) and ∼120 nm (during manipulation) for a single fluorescent semiconductor nanocrystal in a viscous (230 cP) polymer solution.[36,37] Similarly, Cohen et al. reported positioning precision of 550 nm for a 24 nm fluorescent polystyrene bead, 140 nm for a large protein molecule (∼18 nm), and 416 nm for a single organic dye molecule using various software and hardware-based versions of the anti-Brownian electrokinetic (ABEL) trap.[29−33]

Together, plasmonic tweezers, optofluidic tweezers, and electrokinetic trapping methods have focused on pushing the limits of particle trapping toward remarkably smaller particles.[14−23,29−37] These methods are capable of trapping and manipulating particles with dimensions that are generally not accessible to traditional optical tweezers. However, additional features for particle trapping would be desirable, including (1) the ability to isolate and confine individual "target" particles in crowded samples, and (2) the ability to

Received: December 5, 2012
Revised: May 6, 2013
Published: May 17, 2013

actively control and/or exchange the surrounding medium of a confined particle. For example, the manipulation capability of plasmonic and optofluidic nanotweezers are generally limited by the predetermined locations of the nanostructures generating the force fields.[16−20] Furthermore, the electrokinetic trap is capable of isolating a single particle but could be prone to diffusion of other particles into the trapping area.[32]

Particle trapping and manipulation methods based on gentle fluid flow offer several advantages for studying small particles in solution. Contact-free flow-based confinement methods have traditionally relied on microeddies and microvortices, which precludes fine-scale control.[48−52] Recently, we demonstrated a flow-based method for precise point confinement of particles in free solution.[53,54] However, all existing methods for particle trapping lack the ability to dynamically manipulate single objects with high spatial resolution without application of additional external fields.[52]

In this work, we present a new flow-based method for two-dimensional manipulation and high-resolution confinement of single micro- and nanoscale particles in free solution. Single particles are trapped at the stagnation point of a planar extensional flow, and precise control over the position of the stagnation point using automated feedback control enables fine-scale manipulation of particles in two-dimensions. The stagnation point flow is generated in a microfluidic device with a simple cross-slot channel design with two on-chip valves to precisely control fluid flow, thereby enabling particle trapping and manipulation. The stagnation point represents a semistable equilibrium point, where a single target particle is confined and the other particles in solution are simply convected away from the trapping region by fluid flow. Here, we demonstrate facile isolation and confinement of a target particle in a crowded solution. Furthermore, we actively control the surrounding medium of a confined particle by switching the inlet fluid streams in a controlled fashion.

Stagnation point flows are defined by one or multiple regions within a fluid where the local velocity is exactly zero. Planar extensional flow is a stagnation flow containing a single stagnation point at the junction of two laminar streams that converge in opposing directions (Figure 1). In the vicinity of the stagnation point, a planar extensional flow can be expressed as a potential flow with a velocity potential function (φ):

$$\varphi = \left(\frac{\dot{\varepsilon}}{2}\right)(y^2 - x^2) \tag{1}$$

where $\dot{\varepsilon}$ is the strain rate (s^{-1}) and x and y are the particle coordinates with respect to the stagnation point along the inlet and outlet streams, respectively. Equation 1 implies that (*i*) the stagnation point represents a saddle point in the velocity potential, that is, a local minimum (maximum) along the inlet (outlet) streams (Figure 1b); (*ii*) velocity is exactly zero at the stagnation point; $\vec{v}_{(0,0)} = \vec{\nabla}\varphi|_{(0,0)} = \dot{\varepsilon}(-x,y)|_{(0,0)} = (0,0)$. If a particle is precisely positioned at the stagnation point, it will experience zero velocity and is effectively trapped. However, in practice a particle located at a stagnation point will be eventually displaced due to Brownian motion or external fluctuations. Therefore, the stagnation point is a semistable equilibrium point (i.e., saddle point), which is stable (unstable) along the inlet (outlet) streams. In the absence of feedback flow control, particles can only be transiently confined at the stagnation point with finite residence times on the order of the inverse strain rate.[55−58] To achieve stable particle trapping, we implement active flow control along the (unstable) outlet stream to generate an effective trap potential (Figure 1b,c).[53,54,59,60] In this way, the stagnation point position is actively adjusted along the outlet streams in order to effectively confine particles at a predetermined set-point (Supporting Information), albeit without the full translational control.

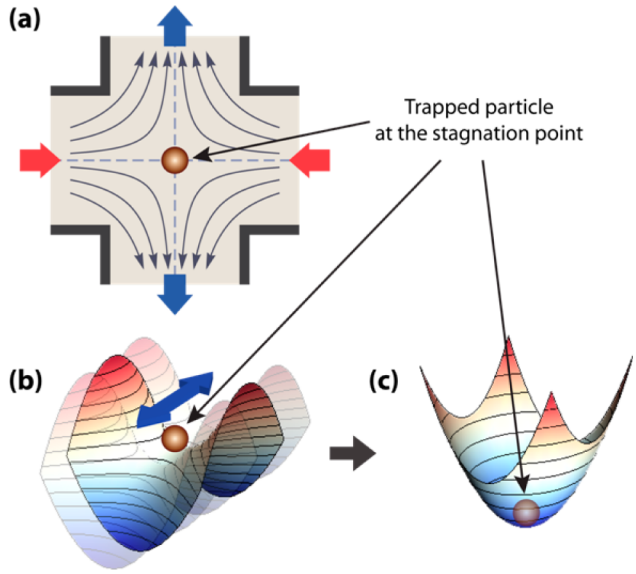

Figure 1. Single particles are confined and manipulated using an automated stagnation point flow generated at a microchannel junction. (a) Two opposing laminar streams meet at the junction, thereby generating a stagnation point where the local fluid velocity is exactly zero. A particle positioned at the stagnation point is effectively trapped. (b,c) A planar extensional flow can be expressed as a potential flow where the stagnation point represents a saddle point in the velocity potential. The stagnation point is a semistable equilibrium point, which is stable (unstable) along the inlet (outlet) streams. By implementing active flow control along the (unstable) outlet streams, a pseudopotential well is created (as shown in (c)) to confine the particle.

In this work, we demonstrate two-dimensional manipulation of particles by implementing simultaneous control of the stagnation point position in orthogonal directions (both along the inlet and outlet streams), thereby significantly increasing the overall versatility of this flow-based confinement method. Two-dimensional manipulation is implemented by precise positioning of the stagnation point along the inlet and outlet streams (Figure 2). Consider two opposing laminar streams (Figure 2a−d, left and right) converging at a microchannel junction, which results in two divergent streams (Figure 2a−d, top and bottom) exiting the junction along the orthogonal axis in opposite directions. The position of the stagnation point at the junction depends on the ratio of the flow rates of the inlet (Q_{left}/Q_{right}) and outlet (Q_{top}/Q_{bottom}) streams.[53] Because of conservation of mass, the stagnation point is located closer to the inlet or outlet stream with the smaller volumetric flow rate. For instance, if the flow rate of the right inlet stream is larger than the left inlet, then the stagnation point will be located closer to the left channel along this axis (Figure 2a,c). In this manner, the stagnation point position can be dynamically controlled by actively adjusting the relative flow rates of the inlet and outlet streams. Two metering valves positioned above the inlet and outlet fluidic channels facilitate the control of the relative flow rates of the inlet and outlet streams, thereby enabling independent control of particle position along each direction (inlet/outlet streams).

dx.doi.org/10.1021/nl4008437 | *Nano Lett.* 2013, 13, 2357−2364

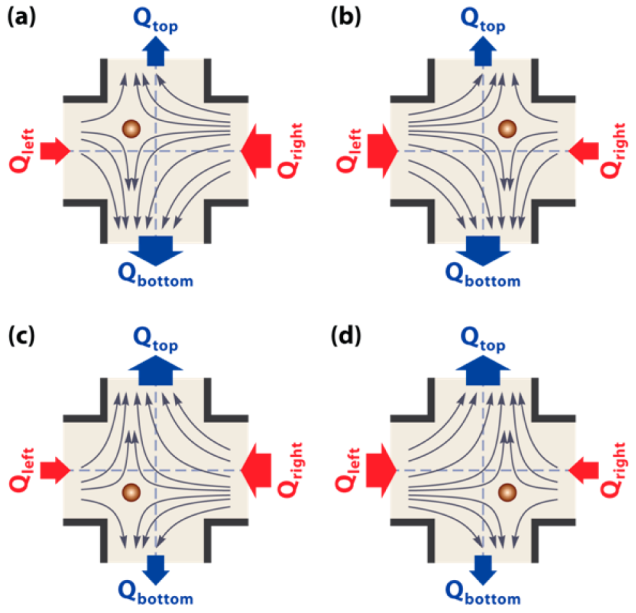

Figure 2. Schematic of the manipulation mechanism for a single particle using an automated stagnation point flow. The position of the stagnation point can be manipulated in two dimensions by changing the relative flow rates of the inlet and outlet streams. As shown in (a) and (b), when the flow rate through the bottom channel is larger than the flow rate through the top channel, the stagnation point lies in the upper half of the junction. Similarly, when the flow rate through the left channel is larger than the right channel, the stagnation point lies in the right half of the junction ((b) and (d)). In this manner, fine-scale control of the stagnation point position enables manipulation of single particles in the microchannel junction.

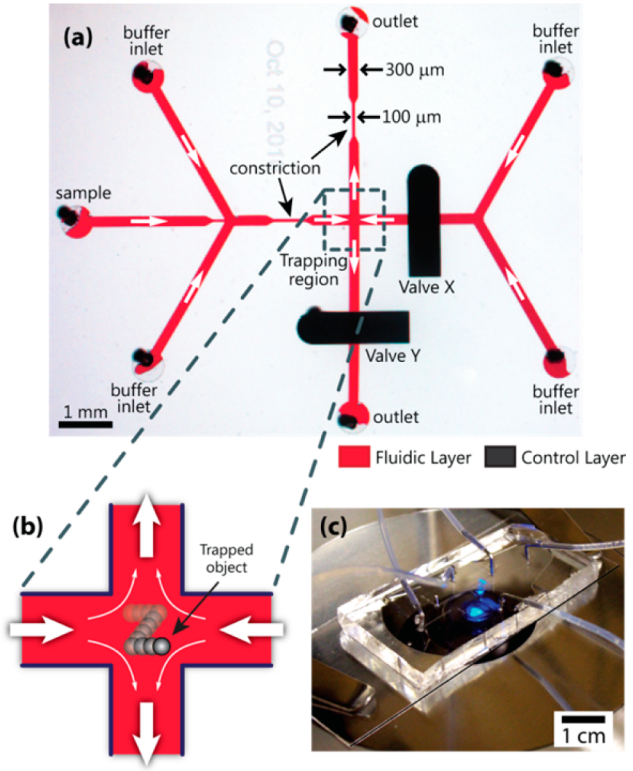

Figure 3. The 2D microfluidic trap. (a) Optical micrograph of a microfluidic manipulation device. Single particles are confined at a predetermined location within the junction of two perpendicular microchannels (trapping region). Two on-chip membrane valves (black) positioned above one inlet channel and one outlet channel are used as metering valves to control the relative flow rates through the opposing channels (red). (b) Schematic of 2D particle trapping. Two opposing laminar streams meet at the intersection of two perpendicular microchannels, thereby creating a well-defined flow field containing a stagnation point where an object is trapped. (c) The microfluidic manipulation device consists of a glass coverslip and a PDMS slab containing the microchannels and valves.

Flow-based confinement and manipulation of micro- and nanoparticles are carried out in a microfluidic device fabricated using multilayer soft lithography (Supporting Information).[61,62] Figure 3a shows a micrograph of the 2D microfluidic trapping device, which consists of a fluidic layer (red) and a control layer (black). Within the fluidic layer, four buffer streams and a sample stream meet at the junction of two perpendicular microchannels (Figure 3a, trapping region) and exit the junction along the outlet channels, thereby generating a planar extensional flow. Fluid flow at the junction is controlled by two monolithic membrane valves (Figure 3a, shown in black, located in the control layer) positioned above one of the inlet and outlet channels. These valves are used as metering valves to control the relative flow rates of the inlet and outlet streams, facilitating fine-scale, two-dimensional control of the stagnation point position at the junction (Figure 3b). Trapping and manipulation of particles is achieved by an automated feedback control algorithm that executes real-time image analysis, particle tracking, and flow field manipulation (Supporting Information). Figure 3c shows a photograph of a microfluidic trapping device mounted on a microscope stage with fluidic connections.

Individual micro- and nanoscale particles can be manipulated in two dimensions within the trapping region by dynamically adjusting the position of the trap center (Figure 4). Using this approach, a particle can be steered toward any arbitrary direction in the lateral plane (along the inlet/outlet streams). As a result, particle trajectories can assume any two-dimensional shape consisting of paths running parallel or diagonal to the inlet/outlet streams. Figure 4a shows the trajectory of a micrometer-sized particle (2.2 μm diameter Nile red fluorescent polystyrene bead) manipulated in the lateral (x–y) plane using the trap. A single particle, initially confined at t = 0, is manipulated in two dimensions to spell out the letter "C". The trajectory is comprised of segments in which the particle moves either parallel or diagonal to the inlet/outlet streams. In this manner, the particle is manipulated along a programmed, predetermined trajectory (shown by arrows) in a 30 μm × 60 μm area with high-precision (RMS accuracy <1 μm). Figure 4b shows the trajectory for a particle spelling out the letter "I" while moving along straight paths parallel to the inlet/outlet streams.

In the 2D hydrodynamic trap, the strain rate $\dot{\epsilon}$ plays a key role on the trap performance. We characterized the effect of strain rate on particle confinement and on the shape of the effective trap potential (Figure 5). Figure 5a shows distinct x–y trajectories for a confined particle (500 nm diameter fluorescent bead) at four different strain rates ($\dot{\epsilon}$ = 2.6–10.3 s^{-1}) with the data organized by rows: $\dot{\epsilon}$ = 2.6 s^{-1} (top row, purple), $\dot{\epsilon}$ = 5.1 s^{-1} (second row, green), $\dot{\epsilon}$ = 7.7 s^{-1} (third row, red), $\dot{\epsilon}$ = 10.3 s^{-1} (bottom row, blue). At each strain rate, the particle is positioned along the inlet stream (x-axis) and trapped at three distinct positions while its trajectory is recorded. For clarity, the intervening trajectory of the particle

dx.doi.org/10.1021/nl4008437 | Nano Lett. 2013, 13, 2357–2364

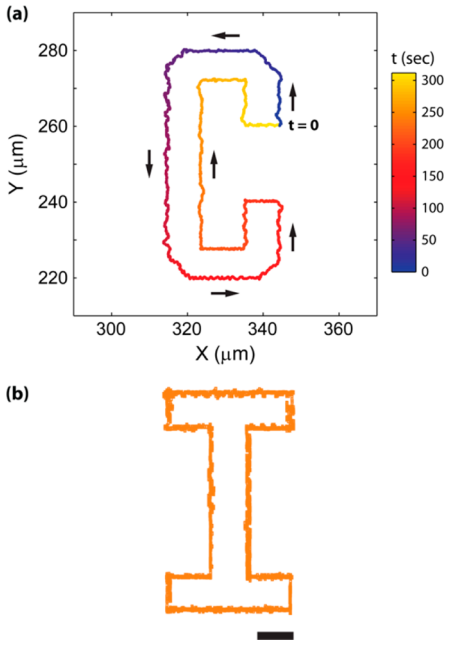

Figure 4. The 2D micromanipulation of single particles using fluid flow. (a) Sample trajectory of a single particle (2.2 μm diameter Nile red fluorescent polystyrene bead) manipulated in two dimensions using the trap. A predetermined trajectory was programmed to spell the letter "C". The manipulation starts at t = 0 and ends when the particle returns to the initial point at t = 300 s. (b) Sample trajectory of an individual particle tracing the letter "I" using the flow-based trapping and manipulation method. Scale bar: 10 μm.

between the three fixed positions is not shown. Figure 5b,c shows the one-dimensional trajectory of a trapped particle at $\dot{\varepsilon}$ = 2.6 s^{-1} along the inlet (x-axis), and outlet (y-axis) streams, respectively. Figure 5d shows a sample two-dimensional trajectory and the corresponding particle displacement histograms for a particle trapped at $\dot{\varepsilon}$ = 7.7 s^{-1}, which corresponds to the trajectory in the dashed box in Figure 5a. Particle confinement along the inlet and outlet streams are characterized by the standard deviations (σ_x = 0.19 μm, σ_y = 0.22 μm) of the Gaussian fits (red curves) to the particle displacement histograms. In this manner, we determined the root-mean-square (RMS) particle displacement from the trap center along the inlet (RMS_X) and outlet (RMS_Y) streams as a function of strain rate (Figure 5e). The RMS particle displacement is <1 μm for all strain rates, generally ranging between 0.16−0.69 μm. In addition, the RMS particle displacement decreases (increases) as the strain rate increases along the inlet (outlet) stream using a constant set of feedback control parameters. Along with the micromanipulation data presented in Figure 4, these results demonstrate high precision confinement and manipulation of micro- and nanoscale particles using the sole action of fluid flow.

By adjusting the fluid strain rate, the effective trap potential for the 2D microfluidic trap can be directly controlled. Figure 6a−d shows histograms of particle displacement from the trap center along the inlet (flow-in) and outlet (flow-out) streams for increasing values of fluid strain rate. Histograms are obtained from the first column of particle trajectories (x = 340 μm) presented in Figure 5a. We define the tightness of confinement as the standard deviation of the Gaussian fit to the histograms, σ_x and σ_y along the inlet and outlet streams, respectively. With increasing strain rate, the tightness of confinement (or trap stiffness) increases along the inlet streams and decreases along the outlet streams. As $\dot{\varepsilon}$ is increased from 5.14 s^{-1} to 10.29 s^{-1}, σ_x drops to half of its initial value (from 0.26 to 0.13 μm), and σ_y increases by 22% (from 0.18 to 0.22 μm). In this manner, trap stiffness along both axes (inlet and outlet) can be tuned with a single flow parameter, namely the fluid strain rate. The shape of the velocity potential function for the planar extensional flow is determined by the strain rate (eq 1). The third column in Figure 6 labeled as "flow potential" shows velocity potential function plots at four different strain rates. The depth of the potential well along the inlet streams increases with the strain rate, thereby resulting in tighter particle confinement along this axis.

Particles are confined along the outlet streams by generating an effective or pseudo potential well via active flow control (Figure 1b,c). The fourth column in Figure 6 shows qualitative 3D plots of the pseudo trap potential as a function of strain rate. The depth of the pseudo potential well along the outlet streams is calculated from experimental data based on the relationship between the velocity potential function and the tightness of confinement along the inlet streams. Delineating the results for σ_x and σ_y presented in the first two columns, these plots indicate that the depth of the effective trap potential increases (decreases) along the inlet (outlet) streams with increasing strain rate.

The effective trap potential is determined by several key parameters, in addition to the strain rate (Supporting Information). Along the inlet streams, a passive trap is formed by fluid flow, and the restoring force arises due to hydrodynamic drag acting on the trapped particle such that $F = \zeta v = (6\pi\eta a)(\dot{\varepsilon}x) = \kappa_{inlet}x$, where η is the viscosity of the medium, a is particle radius (or hydrodynamic radius), $\dot{\varepsilon}$ is strain rate, and x is the distance between the particle and the trap center along the inlet streams. In this way, the trap stiffness along the inlet streams is $\kappa_{inlet} = 6\pi\eta a\dot{\varepsilon}$. The equipartition theorem can be used to determine the RMS particle displacement from trap center (RMS_X) along the inlet streams, such that $RMS_X = (kT/\kappa_{inlet})^{1/2}$. Estimates of the particle displacement along the inlet streams (RMS_X) are in good agreement with the experimentally determined values (Figure 5e).

Along the outlet streams, however, a pseudopotential well is generated by active flow control, which complicates the analytical expression for trap stiffness. The RMS particle displacement from trap center along the outlet streams ($RMS_Y = (kT/\kappa_{outlet})^{1/2}$) is determined by a balance between convection (i.e., fluid strain rate $\dot{\varepsilon}$), Brownian motion (i.e., ambient temperature, viscosity of the medium, hydrodynamic radius), and the type of the feedback controller and the associated control parameters (i.e., gain constants, feedback delay). The effective trap potential along the outlet streams dictates the particle size limit for hydrodynamic trapping, which is the smallest particle that can be confined and manipulated. Using the current set of flow and feedback control parameters (proportional-only controller), we estimate that the particle size limit is ~30 nm (Supporting Information). However, we anticipate that even smaller nanoparticles can be confined by implementing advanced feedback controllers (e.g., PID controllers) using the same experimental setup and a similar set of fluid strain rates.

Finally, we demonstrate two distinct features of the flow-based trapping method described in this work. First, we directly show the isolation of a single target particle within a crowded particle solution (Figure 7). In general, trapping methods based

dx.doi.org/10.1021/nl4008437 | Nano Lett. 2013, 13, 2357−2364

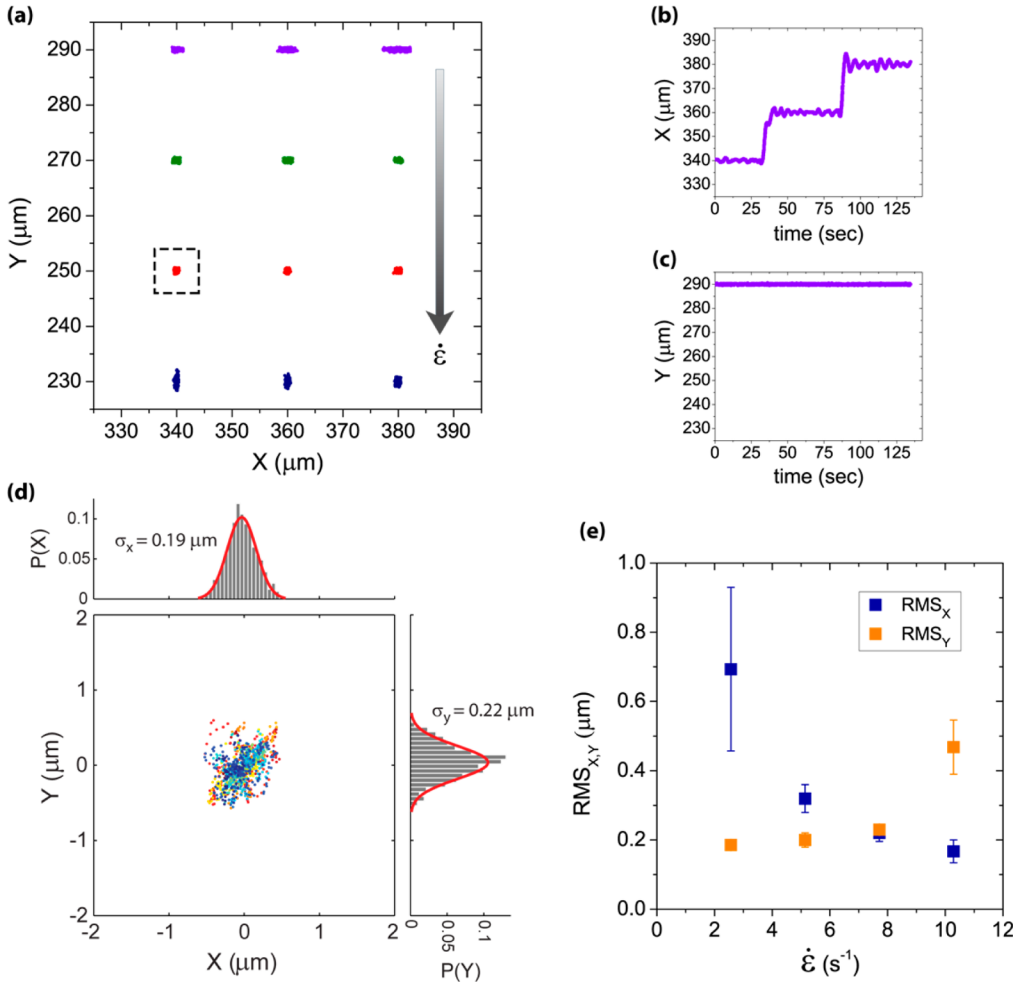

Figure 5. Characterization of trap response. (a) Particle trajectories at four different strain rates. Top row: $\dot{\varepsilon} = 2.6\ s^{-1}$ (purple), second row: $\dot{\varepsilon} = 5.1\ s^{-1}$ (green), third row: $\dot{\varepsilon} = 7.7\ s^{-1}$ (red), bottom row: $\dot{\varepsilon} = 10.3\ s^{-1}$ (blue). At each strain rate, a single particle (500 nm diameter bead) is confined at three distinct positions along the inlet streams (*x*-axis). For clarity, the intervening trajectories between the three trapping positions are not shown. Particle trajectory along (b) the inlet and (c) the outlet streams at strain rate, $\dot{\varepsilon} = 2.6\ s^{-1}$ (first row in (a) shown in purple). (d) Two-dimensional center-of-mass positions and the corresponding displacement histograms for the boxed trajectory in (a) at $\dot{\varepsilon} = 7.7\ s^{-1}$. The standard deviation of particle displacement is <1 μm ($\sigma_x = 0.19\ \mu$m, $\sigma_y = 0.22\ \mu$m). (e) Effect of strain rate $\dot{\varepsilon}$ on particle displacement from the trap center along the inlet (RMS_X) and outlet (RMS_Y) streams.

on passive force fields are prone to unintentional capture of particles adjacent to the trap center. Trapping methods based on active feedback (e.g., electrokinetic trapping methods) can achieve isolation of a target particle within a crowded solution, but random diffusion of particles into the trapping area can hamper this in practice. Because of the semistable nature of the stagnation point, hydrodynamic trapping intrinsically allows for isolation and confinement of a single target particle, such that untrapped particles in the sample are convected away by fluid flow. To demonstrate this feature, we introduced a solution of fluorescent polystyrene beads into the trapping area through the sample inlet (see Figure 3). Next, the sample inlet stream was closed, and a single target particle was isolated and trapped from this sample (Figure 7a). Untrapped particles in the sample are cleared from the trapping area via fluid flow through the buffer inlets. In this manner, a single trapped particle is effectively trapped and isolated from the rest of the sample within approximately 25 s. For the device shown in Figure 7a, single target particles entering the trapping region within a 100 × 100 μm area centered at the microchannel junction (300 × 300 μm) can be specifically captured and manipulated. Membrane valves with enhanced flow control capacity would extend the manipulation area, and enable control over all particles passing through the trapping region.[53]

A second key advantage of hydrodynamic trapping is the ability to actively and precisely control the surrounding medium of a trapped object. As an experimental proof-of-principle demonstration, we trapped a single fluorescein-coated polystyrene bead (1.9 μm diameter), and we periodically switched the medium surrounding the trapped particle between pH 4 and pH 8 buffers (citric acid − Na_2HPO_4) in a predefined manner. The fluorescence emission from the bead is observed as a function of time during the medium exchange (Figure 7b). Fluorescein is a highly pH sensitive dye, and its fluorescence emission decreases with pH (maximum quantum yield at pH 9.5 that significantly decreases at lower pH). As a result, the fluorescence emission intensity fluctuates between higher and lower values as the trapped bead is transiently immersed into high and low pH buffer solutions, respectively (inset, Figure 7b left panel). Importantly, the fluctuations in the fluorescence emission intensity directly correlate to the changes in the surrounding medium pH (Figure 7b). During the observation

dx.doi.org/10.1021/nl4008437 | *Nano Lett.* 2013, 13, 2357−2364

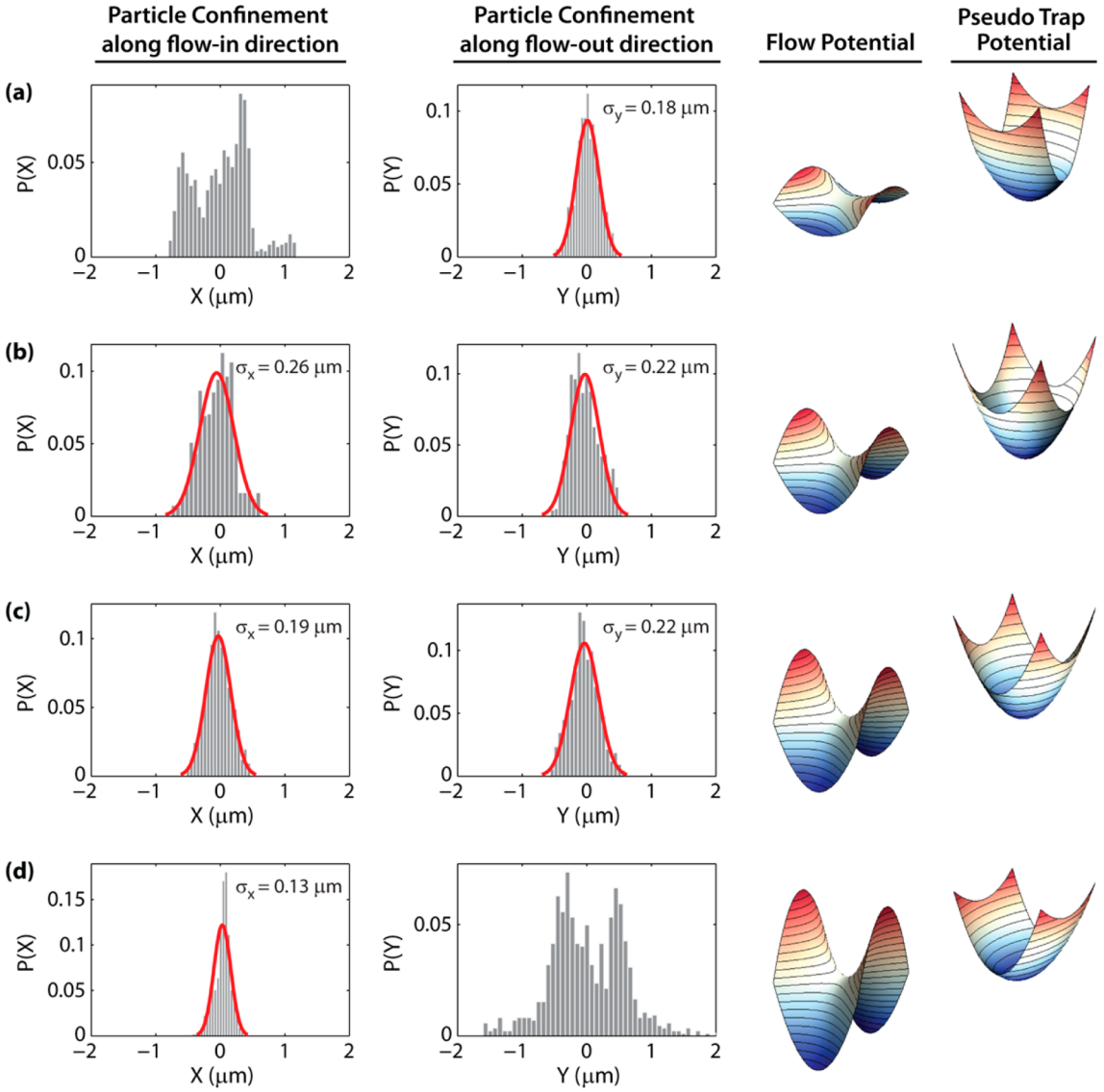

Figure 6. Shaping the effective potential of the 2D microfluidic trap for a 500 nm bead. The two columns on the left show the distribution of particle displacement from the trap center along the inlet (X) and outlet (Y) streams at four different strain rates: (a) $\dot{\varepsilon}$ = 2.6 s^{-1}, (b) $\dot{\varepsilon}$ = 5.1 s^{-1}, (c) $\dot{\varepsilon}$ = 7.7 s^{-1}, and (d) $\dot{\varepsilon}$ = 10.3 s^{-1}. In each case, the trap centers (X,Y) = (0,0) correspond to individual particle positions displayed in the first column of Figure 5a. The standard deviations (σ_x and σ_y) are obtained by fitting a Gaussian function (red curves) to the particle displacement data. Upon increasing the strain rate, the width of the distributions decreases (increases) along the inlet (outlet) streams. In the third column, the flow potential for the planar extensional flow as a function of strain rate is shown. In the fourth column, the effective trap potential for a 500 nm particle using the automated trap is shown. The shape of the pseudo potential well can be "tuned" by varying the strain rate.

period, the fluorescein molecules on the bead surface gradually photobleach, which results in an overall steady decrease of fluorescence intensity. We further demonstrate that we can control the period of medium exchange. For the two traces shown in Figure 7b, we carried out buffer exchange at two different periods (T = 40 and 60 s, respectively for the left and the right panel), which show excellent agreement with the period of fluorescence emission intensity fluctuations. The results depicted in Figure 7b demonstrate a critical advantage of flow-based trapping. Among existing trapping methods, optical tweezers have also been shown to allow for replacement of solution medium in real time, albeit using large particles confined by high-intensity laser beams.[63]

In this work, we report a new method for full two-dimensional manipulation and confinement of micro- and nanoscale particles using the sole action of fluid flow. By coupling an automated feedback controller with a stagnation point flow field, we demonstrate 2D manipulation of single particles at a microchannel junction via fine-scale adjustment of fluid flow using two integrated, on-chip metering valves. The microfluidic trap described here offers a versatile platform for nonperturbative observation and analysis of single micro- and nanoparticles in free solution in the absence of electric, magnetic, optical, and acoustic force fields. Similar to electrokinetic trapping methods, the flow-based method has an effective spring constant that scales linearly with particle size and viscosity of the medium, which offers the possibility for facile trapping of small nanoparticles in free solution. This method is amenable to virtually any particle that can be visualized, and therefore may expand the potential applications of micro/nanomanipulation tools. By employing the intrinsic advantages of fluid flow, this new powerful approach may open

dx.doi.org/10.1021/nl4008437 | *Nano Lett.* 2013, 13, 2357−2364

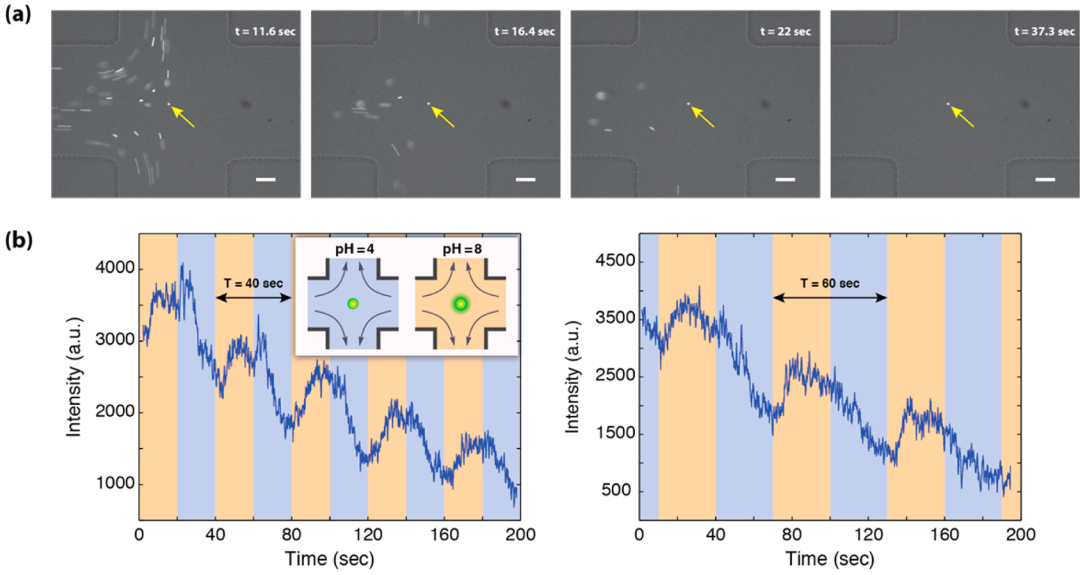

Figure 7. (a) Isolation and confinement of a single particle from a crowded solution using the hydrodynamic trap. A solution containing fluorescent polystyrene beads (2.2 μm diameter) is introduced to the trapping area. One of the beads is effectively isolated and confined using the hydrodynamic trap, and the remainder of the untrapped beads in the sample is convected away by fluid flow within approximately 25 s following sample introduction. Yellow arrow shows the position of the trapped particle. Scale bar: 50 μm. (b) Dynamic control of the surrounding medium of a trapped particle. A single fluorescein-coated polystyrene bead (1.9 μm diameter) is trapped, and the surrounding medium is periodically exchanged in a preprogrammed manner between high pH (pH 8) and low pH (pH 4) buffer solutions. The intensity of fluorescence emission from the pH sensitive dye (fluorescein) fluctuates as the surrounding medium changes, thereby demonstrating the effectiveness of the buffer exchange in the trap.

up new venues for the study of biomolecules, micro- and nanoscale particles, and cells.

■ ASSOCIATED CONTENT

Ⓢ Supporting Information

A description of the feedback control mechanism, key performance parameters, device fabrication and experimental setup for the hydrodynamic trap, and a movie showing particle trapping and manipulation using the hydrodynamic trap. This material is available free of charge via the Internet at http://pubs.acs.org.

■ AUTHOR INFORMATION

Corresponding Author

*E-mail: cms@illinois.edu.

Notes

The authors declare no competing financial interest.

■ ACKNOWLEDGMENTS

We thank Professor Paul J. A. Kenis and his group for providing access to cleanroom facilities for microdevice fabrication. This work was supported by a Packard Fellowship from the David and Lucile Packard Foundation and an NIH Pathway to Independence (PI) Award (4R00HG004183-03).

■ REFERENCES

(1) Johann, R. M. *Anal. Bioanal. Chem.* **2006**, *385* (3), 408−412.
(2) Nilsson, J.; Evander, M.; Hammarstrom, B.; Laurell, T. *Anal. Chim. Acta* **2009**, *649* (2), 141−157.
(3) Yi, C. Q.; Li, C. W.; Ji, S. L.; Yang, M. S. *Anal. Chim. Acta* **2006**, *560* (1−2), 1−23.
(4) Ashkin, A. *Proc. Natl. Acad. Sci. U.S.A.* **1997**, *94* (10), 4853−4860.
(5) Grier, D. G. *Nature* **2003**, *424* (6950), 810−816.
(6) Dholakia, K.; Cizmar, T. *Nat. Photonics* **2011**, *5* (6), 335−342.
(7) Chiou, P. Y.; Ohta, A. T.; Wu, M. C. *Nature* **2005**, *436* (7049), 370−372.
(8) Uhrig, K.; Kurre, R.; Schmitz, C.; Curtis, J. E.; Haraszti, T.; Clemen, A. E. M.; Spatz, J. P. *Lab Chip* **2009**, *9* (5), 661−668.
(9) Hansen, P. M.; Bhatia, V. K.; Harrit, N.; Oddershede, L. *Nano Lett.* **2005**, *5* (10), 1937−1942.
(10) Urban, A. S.; Lutich, A. A.; Stefani, F. D.; Feldmann, J. *Nano Lett.* **2010**, *10* (12), 4794−4798.
(11) Pang, Y.; Gordon, R. *Nano Lett.* **2012**, *12* (1), 402−406.
(12) Balijepalli, A.; Gorman, J. J.; Gupta, S. K.; LeBrun, T. W. *Nano Lett.* **2012**, *12* (5), 2347−2351.
(13) Sainidou, R.; García de Abajo, F. J. *Phys. Rev. Lett.* **2008**, *101* (13), 136802.
(14) Yang, A. H. J.; Moore, S. D.; Schmidt, B. S.; Klug, M.; Lipson, M.; Erickson, D. *Nature* **2009**, *457* (7225), 71−75.
(15) Kang, P.; Serey, X.; Chen, Y.-F.; Erickson, D. *Nano Lett.* **2012**, *12* (12), 6400−6407.
(16) Chen, Y.-F.; Serey, X.; Sarkar, R.; Chen, P.; Erickson, D. *Nano Lett.* **2012**, *12* (3), 1633−1637.
(17) Mandal, S.; Serey, X.; Erickson, D. *Nano Lett.* **2009**, *10* (1), 99−104.
(18) Chen, C.; Juan, M. L.; Li, Y.; Maes, G.; Borghs, G.; Van Dorpe, P.; Quidant, R. *Nano Lett.* **2012**, *12* (1), 125−132.
(19) Wang, K.; Schonbrun, E.; Steinvurzel, P.; Crozier, K. B. *Nat. Commun* **2011**, *2*, 469.
(20) Roxworthy, B. J.; Ko, K. D.; Kumar, A.; Fung, K. H.; Chow, E. K. C.; Liu, G. L.; Fang, N. X.; Toussaint, K. C. *Nano Lett.* **2011**, *12* (2), 796−801.
(21) Roxworthy, B. J.; Toussaint, K. C. *Sci. Rep.* **2012**, 2.
(22) Yang, X.; Liu, Y.; Oulton, R. F.; Yin, X.; Zhang, X. *Nano Lett.* **2011**, *11* (2), 321−328.
(23) Saleh, A. A. E.; Dionne, J. A. *Nano Lett.* **2012**, *12* (11), 5581−5586.
(24) Schnelle, T.; Hagedorn, R.; Fuhr, G.; Fiedler, S.; Muller, T. *Biochim. Biophys. Acta* **1993**, *1157* (2), 127−140.
(25) Muller, T.; Gradl, G.; Howitz, S.; Shirley, S.; Schnelle, T.; Fuhr, G. *Biosens. Bioelectron.* **1999**, *14* (3), 247−256.
(26) Fiedler, S.; Shirley, S. G.; Schnelle, T.; Fuhr, G. *Anal. Chem.* **1998**, *70* (9), 1909−1915.
(27) Green, N. G.; Morgan, H.; Milner, J. J. *J. Biochem. Biophys. Methods* **1997**, *35* (2), 89−102.

(28) Rosenthal, A.; Voldman, J. *Biophys. J.* **2005**, *88* (3), 2193−2205.
(29) Cohen, A. E. *Phys. Rev. Lett.* **2005**, *94* (11), 118102.
(30) Cohen, A. E.; Moerner, W. E. *Appl. Phys. Lett.* **2005**, *86*, 9.
(31) Cohen, A. E.; Moerner, W. E. *Proc. Natl. Acad. Sci. U.S.A.* **2006**, *103* (12), 4362−4365.
(32) Cohen, A. E.; Moerner, W. E. *Opt. Express* **2008**, *16* (10), 6941−6956.
(33) Fields, A. P.; Cohen, A. E. *Proc. Natl. Acad. Sci. U.S.A.* **2011**, *108* (22), 8937−8942.
(34) Armani, M.; Chaudhary, S.; Probst, R.; Walker, S.; Shapiro, B. *Int. J. Robust. Nonlin. Control* **2005**, *15* (16), 785−803.
(35) Armani, M. D.; Chaudhary, S. V.; Probst, R.; Shapiro, B. *J. Microelectromech. Syst.* **2006**, *15* (4), 945−956.
(36) Ropp, C.; Probst, R.; Cummins, Z.; Kumar, R.; Berglund, A. J.; Raghavan, S. R.; Waks, E.; Shapiro, B. *Nano Lett.* **2010**, *10* (7), 2525−2530.
(37) Ropp, C.; Cummins, Z.; Probst, R.; Qin, S.; Fourkas, J. T.; Shapiro, B.; Waks, E. *Nano Lett.* **2010**, *10* (11), 4673−4679.
(38) Guan, W. H.; Joseph, S.; Park, J. H.; Krstić, P. S.; Reed, M. A. *Proc. Natl. Acad. Sci. U.S.A.* **2011**, *108* (23), 9326−9330.
(39) Celebrano, M.; Rosman, C.; Sönnichsen, C.; Krishnan, M. *Nano Lett.* **2012**, *12* (11), 5791−5796.
(40) Gosse, C.; Croquette, V. *Biophys. J.* **2002**, *82* (6), 3314−3329.
(41) Lee, H.; Purdon, A. M.; Westervelt, R. M. *Appl. Phys. Lett.* **2004**, *85* (6), 1063−1065.
(42) Mirowski, E.; Moreland, J.; Zhang, A.; Russek, S. E.; Donahue, M. J. *Appl. Phys. Lett.* **2005**, *86* (24), 3.
(43) Ding, X. Y.; Lin, S. C. S.; Kiraly, B.; Yue, H. J.; Li, S. X.; Chiang, I. K.; Shi, J. J.; Benkovic, S. J.; Huang, T. J. *Proc. Natl. Acad. Sci. U.S.A.* **2012**, *109* (28), 11105−11109.
(44) Shi, J. J.; Ahmed, D.; Mao, X.; Lin, S. C. S.; Lawit, A.; Huang, T. J. *Lab Chip* **2009**, *9* (20), 2890−2895.
(45) Hertz, H. M. *J. Appl. Phys.* **1995**, *78* (8), 4845−4849.
(46) Evander, M.; Johansson, L.; Lilliehorn, T.; Piskur, J.; Lindvall, M.; Johansson, S.; Almqvist, M.; Laurell, T.; Nilsson, J. *Anal. Chem.* **2007**, *79* (7), 2984−2991.
(47) Neuman, K. C.; Block, S. M. *Rev. Sci. Instrum.* **2004**, *75* (9), 2787−2809.
(48) Lutz, B. R.; Chen, J.; Schwartz, D. T. *Anal. Chem.* **2006**, *78* (15), 5429−5435.
(49) Chiu, D. *Anal. Bioanal. Chem.* **2007**, *387* (1), 17−20.
(50) Lieu, V. H.; House, T. A.; Schwartz, D. T. *Anal. Chem.* **2012**, *84* (4), 1963−1968.
(51) Lin, C. M.; Lai, Y. S.; Liu, H. P.; Chen, C. Y.; Wo, A. M. *Anal. Chem.* **2008**, *80* (23), 8937−8945.
(52) Petit, T.; Zhang, L.; Peyer, K. E.; Kratochvil, B. E.; Nelson, B. J. *Nano Lett.* **2012**, *12* (1), 156−160.
(53) Tanyeri, M.; Ranka, M.; Sittipolkul, N.; Schroeder, C. M. *Lab Chip* **2011**, *11* (10), 1786−1794.
(54) Tanyeri, M.; Johnson-Chavarria, E. M.; Schroeder, C. M. *Appl. Phys. Lett.* **2010**, *96* (22), 224101.
(55) Dylla-Spears, R.; Townsend, J. E.; Jen-Jacobson, L.; Sohn, L. L.; Muller, S. J. *Lab Chip* **2010**, *10* (12), 1543−1549.
(56) Schroeder, C. M.; Babcock, H. P.; Shaqfeh, E. S. G.; Chu, S. *Science* **2003**, *301* (5639), 1515−1519.
(57) Perkins, T. T.; Smith, D. E.; Chu, S. *Science* **1997**, *276* (5321), 2016−2021.
(58) Haward, S. J.; Oliveira, M. S. N.; Alves, M. A.; McKinley, G. H. *Phys. Rev. Lett.* **2012**, *109* (12), 128301.
(59) Curtis, M. D.; Sheard, G. J.; Fouras, A. *Lab Chip* **2011**, *11* (14), 2343−2351.
(60) Hu, Y. T.; Pine, D. J.; Leal, L. G. *Phys. Fluids* **2000**, *12* (3), 484−489.
(61) Unger, M. A.; Chou, H. P.; Thorsen, T.; Scherer, A.; Quake, S. R. *Science* **2000**, *288* (5463), 113−116.
(62) Whitesides, G. M.; Ostuni, E.; Takayama, S.; Jiang, X. Y.; Ingber, D. E. *Annu. Rev. Biomed. Eng.* **2001**, *3*, 335−373.
(63) Perkins, T.; Smith, D.; Larson, R.; Chu, S. *Science* **1995**, *268* (5207), 83−87.